communications biology

A Nature Portfolio journal

Article

https://doi.org/10.1038/s42003-025-08589-5

The low-fidelity DNA Pol IV accelerates evolution of pathogenicity genes in *Pseudomonas aeruginosa*

Sofía D. Castell[1,2], Consuelo M. Fernandez[1,6], Ignacio N. Tumas[1,6], Lucía M. Margara[1], María C. Miserendino[1,3], Danilo G. Ceschin[4], Roberto J. Pezza[5] & Mariela R. Monti[1]

Specialized DNA polymerases facilitate various cellular processes. Despite extensive research, the mutagenic effects of these error-prone enzymes on genomes are not fully understood. Here we show that Pol IV promotes genomic instability in *Pseudomonas aeruginosa* by misincorporating oxidized guanine nucleotides. This activity led to a distinctive mutational signature, characterized by A-to-C transversions occurring preferentially at AT sites flanked by a 5'G and/or 3'C. Furthermore, Pol IV preferentially targeted pathogenicity genes located at specific chromosomal locations near the replication termination region and rRNA-encoding operons. Half of the mutation events catalyzed by Pol IV impaired gene function. This can be attributed to the bias of Pol IV for mutating codons with its preferred sequence contexts, leading to substitutions to unreactive alanine and glycine residues. Remarkably, mutation signatures identified for Pol IV were found in clinical isolate genomes of *P. aeruginosa*, providing compelling evidence for its role in genetic diversification during pathogen adaptation.

Mutations are prominent sources of genetic diversity, impacting adaptation, evolution and tumorigenesis. While often viewed as a stochastic process, there is increasing evidence that mutations can also exhibit strong biases[1]. These biases have been linked to mutagenic mechanisms at play and genomic features that influence mutation processes[1,2]. Different mutational processes produce distinctive combinations of mutation types and specific context-dependent patterns, referred to as mutational signatures. Importantly, identifying the mutagenic processes underlying a mutational signature is essential for predicting adaptive outcomes in pathogenic bacteria.

Errors made by DNA polymerases (Pol) during replication are important contributors to mutagenesis and genomic instability. High-fidelity replicative Pols carry out most of the DNA synthesis required for genome duplication[3,4]. These enzymes achieve accurate replication by discriminating between correct nucleotides during polymerization and correcting errors through proofreading. In addition, overall fidelity is maintained by the mismatch repair (MMR) system[5]. Mismatches uncorrected by proofreading are recognized by the MutS repair protein, which subsequently recruits MutL to remove the newly synthesized strand containing the incorrect nucleotide.

Faithful DNA replication by replicative Pols can be challenged upon encountering template lesions or difficult-to-replicate regions[6]. Since stalled replication forks can threaten cell viability, replicative Pols rely on specialized translesion synthesis (TLS) Pols to continue DNA replication[3,4,6]. TLS Pols inherently exhibit lower accuracy compared to replicative Pols due to their lack of intrinsic proofreading activity and a more open active site architecture[3,4]. Consequently, their ability to relieve replication stall often comes at the price of increased mutagenesis.

Most organisms possess a wide repertoire of TLS Pols dedicated to specific roles. Among these, Pol IV is conserved across all life domains. The mutagenic potential of this Y-family DNA Pol has been well-established in vitro. Both Pol IV and its eukaryotic homolog, Pol κ, catalyze the misincorporation of oxidized nucleotides and low-fidelity replication of undamaged DNA[7–9]. Additionally, Pol IV promotes genetic diversity during stationary-phase and under the SOS DNA-damage response[10–13]. While Pol

[1]Centro de Investigaciones en Química Biológica de Córdoba (CIQUIBIC), CONICET, Departamento de Química Biológica Ranwel Caputto, Facultad de Ciencias Químicas, Universidad Nacional de Córdoba, Córdoba, Argentina. [2]Centro de Investigación en Bioquímica Clínica e Inmunología (CIBICI), CONICET, Departamento de Bioquímica Clínica, Facultad de Ciencias Químicas, Universidad Nacional de Córdoba, Córdoba, Argentina. [3]Institute of Science and Technology Austria, Klosterneuburg, Austria. [4]Centro de Investigación en Medicina Traslacional "Severo R. Amuchástegui" (CIMETSA), CONICET, Instituto Universitario de Ciencias Biomédicas de Córdoba (IUCBC), Córdoba, Argentina. [5]Cell Cycle and Cancer Biology Research Program, Oklahoma Medical Research Foundation, Oklahoma City, OK, USA. [6]These authors contributed equally: Consuelo M. Fernandez, Ignacio N. Tumas. e-mail: mariela.monti@unc.edu.ar

IV is crucial for stress-induced mutagenesis, it does not significantly contribute to genetic diversity under normal growth conditions. The loss of Pol IV does not affect the rate or spectra of genomic mutations in unstressed bacterial cells[10,14–19], suggesting tight regulation of Pol IV-promoted mutagenesis under normal conditions that breaks down during stress.

Several regulatory mechanisms limit DNA synthesis by TLS Pols[3]. A key regulatory point involves their interaction with processivity sliding clamps, which provide a topological link to the DNA template and localize to DNA replication sites[20]. In this context, our previous research revealed a non-canonical function of MutS in modulating the association of Pol IV with β clamp[16]. According to our model, Pol IV can effectively alleviate stalling of the replication fork; however, if it incorporates an erroneous nucleotide, MutS recognizes the mispair and disrupts the Pol IV-β clamp interaction. This action by MutS restricts further replication by Pol IV and promotes the removal of the incorrect nucleotide through the proofreading activity of a high-fidelity Pol.

Although Pol IV has been extensively studied, its influence on mutagenesis across genomes remains poorly understood. To address this knowledge gap, we examined the Pol IV-mutational profile at the genomic level in *Pseudomonas aeruginosa*. This opportunistic pathogen transitions from acute virulent to host-adapted states in chronic lung infections in Cystic Fibrosis patients[21,22]. This adaptation is primarily mediated by inactivating mutations that turn off acute virulence factors, such as motility appendages and pigments, in response to selective pressures, including the highly oxidative environment of the Cystic Fibrosis lung[21–23].

Results

Pol IV mutagenesis is associated with the misincorporation of oxidized nucleotides

We previously established that *P. aeruginosa* MutS interaction with β clamp is critical for controlling Pol IV mutagenesis[16]. Pol IV contributes to spontaneous mutagenesis in a *mutS*$^{\beta}$ (S$^{\beta}$) PAO1 mutant strain, which expresses a MutS version unable to bind to β clamp, but not in the PAO1 (WT) strain (Supplementary Fig. 1A). Briefly, S$^{\beta}$ exhibited a high proportion of AT>CG substitutions in the chromosomal *nfxB* gene, which encodes a repressor of the *mexCD-oprJ* efflux genes. Deletion of the Pol IV-encoding *dinB* gene decreased AT>CG rates in S$^{\beta}$ (*mutS*$^{\beta}$ *dinB* strain, S$^{\beta}$D); however, it did not change the mutation *nfxB* spectra in WT (*dinB* strain, D).

AT>CG transversions can result from the incorporation of 8-oxo-2'-deoxyguanosine-5'-triphosphate (oxodGTP) opposite a template adenine, a process Pol IV can catalyze in vitro. Therefore, we hypothesized that MutS regulates Pol IV mutagenesis associated with misinsertion of oxodGTP. To test this, we estimated mutation rates in cells treated with the free-radical producing agent paraquat (Fig. 1A, Supplementary Fig. 1B, and Supplementary Tables 1 and 2). S$^{\beta}$ cells exposed to a non-lethal paraquat concentration showed a 2-fold increment in mutation rates to resistance to ciprofloxacin (*nfxB* is mutated, Cip^{r}) and amikacin (different target genes are mutated, Amk^{r}) relative to untreated cells. In contrast, paraquat did not affect the mutation rates in the S$^{\beta}$D, WT and D strains.

We next estimated mutation rates in exponentially growing *mutT* (T), *mutT mutS*$^{\beta}$ (TS$^{\beta}$), *mutT dinB* (TD) and *mutT mutS*$^{\beta}$ *dinB* (TS$^{\beta}$D) cells in liquid cultures (Fig. 1B, Supplementary Fig. 1C and Supplementary Table 3). The deficiency of MutT, which hydrolyzes oxodGTP[24], should increase oxodGTP levels and promote its DNA incorporation by Pol IV. Consistent with previous data[25], T showed 100–1000 higher mutation rates relative to WT. TS$^{\beta}$ displayed a 3- to 5-fold increase in mutation rates to resistance to rifampicin (*rpoB* is mutated, Rif^{r}), Cip^{r} and Amk^{r} relative to T. The Pol IV-deficient strain, TS$^{\beta}$D, exhibited a decrease in these mutation rates compared to TS$^{\beta}$, indicating that Pol IV can target the Rif^{r}, Cip^{r} and Amk^{r} genes. Conversely, deficiency of Pol IV in T did not affect mutation rates.

To confirm that Pol IV is involved in the increased mutagenesis in TS$^{\beta}$, we performed complementation assays by introducing arabinose-inducible p5BAD plasmids bearing wild-type and mutant *dinB* alleles into TS$^{\beta}$D (Supplementary Fig. 1D and Supplementary Table 4). Pol IV expression from plasmid p5BAD-*dinB* increased mutation rates 2-fold relative to cells harboring the empty vector p5BAD or the p5BAD-*dinB*D8A derivative, encoding the inactive DNA polymerase Pol IV-D8A mutant[15].

We also measured mutation rates in colony-grown cells (Supplementary Fig. 2 and Supplementary Table 5) to evaluate if Pol IV contributes to mutagenesis in this condition, as mutation accumulation experiments (described below) involved colony streaking. Pol IV-mediated mutagenesis differed between cells in liquid cultures and colonies, indicating that the activity of this enzyme depends on the physiological state of the cell. Compared to T, TS$^{\beta}$ exhibited a 12- and 7-fold increase in Cip^{r} and Amk^{r} mutation rates, respectively, and no significant differences in Rif^{r} mutation rates. Deletion of *dinB* only decreased the mutation rate to Cip^{r} in TS$^{\beta}$, indicating that Pol IV is involved in the mutagenesis of *nfxB*, but not of genes associated with Amk^{r} and Rif^{r}. No significant differences in mutation rates were detected among T and TD.

In summary, our findings demonstrate that Pol IV-mediated mutagenesis involves the erroneous incorporation of oxodGTP into DNA, and this activity is regulated by MutS through its interaction with β clamp.

Pol IV generates highly inactive variants of the reporter *nfxB* gene

Loss-of-function mutations are a common adaptation in *P. aeruginosa* during cystic fibrosis airway infections. To ascertain whether Pol IV produces inactivating mutations, we evaluated the repressor activity of NfxB variants obtained from Cip^{r} clones of WT, S$^{\beta}$, D and S$^{\beta}$D (Figs. 1C and 1D, Supplementary Fig. 3A, and Supplementary data 1). Inactivating mutations within *nfxB* impair NfxB repressor activity, leading to overexpression of the MexCD-OprJ efflux pump and Cip^{r}[26]. To measure the repressor activity of NfxB variants, we integrated a transcriptional fusion of the *mexC* promoter to the *luxCDABE* operon in the chromosome of the PAO1 strains[27]. Loss-of-function mutations in *nfxB* de-repress *luxCDABE* expression, increasing luminescence.

Cip^{r} clones from S$^{\beta}$ expressed NfxB variants showing a high (29%) or medium (63%) inactivation level. These highly inactivated NfxB variants were not detected in S$^{\beta}$D, which showed Cip^{r} clones with a medium (39%) and low (61%) inactivation level. In WT, 81% of Cip^{r} clones exhibited medium luminescence levels while 19% showed low levels. A similar proportion was observed in D.

A significant positive correlation was observed between luminescence intensity and ciprofloxacin resistance levels in clones from all strains (Spearman correlation coefficients: 0.57-0.70) (Supplementary Fig. 3B). Furthermore, sequencing of *nfxB* in four S$^{\beta}$ clones with the highest luminescence levels revealed missense mutations that affected CTG codons (AT > CG), leading to leucine-to-arginine substitutions (Leu14Arg, Leu29Arg, Leu40Arg, and Leu147Arg). These results confirmed the inactivation of the chromosomal *nfxB* gene.

All these findings indicate that Pol IV efficiently generates highly inactive NfxB variants in S$^{\beta}$. As expected from the fact that Pol IV does not contribute to spontaneous mutagenesis in WT, there were no differences in the kind of variants detected among WT and D.

Impact of Pol IV activity on spontaneous mutations throughout the genome

The AT>CG transversion dominates the mutation spectra in the *mutT* strains. To assess the mutator activity of Pol IV at the genome-wide level, we conducted mutation accumulation experiments. This involved propagating 8 independent lines derived from T, TS$^{\beta}$, TD and TS$^{\beta}$D through single-individual bottlenecks, achieved by daily streaking for single colonies over 100 consecutive days (Fig. 2A). This experiment was repeated twice, resulting in 16 lines per strain. After each line underwent ~2650 generations during the 100-day experiment, we identified mutations by sequencing the genomes of 8–14 lines and the corresponding ancestor. We anticipated observing Pol IV mutagenesis in TS$^{\beta}$ due to loss of MutS regulation, but not in T, where the MutS control mechanism is operating. Conversely, predicting outcomes in TD and TS$^{\beta}$D is challenging, as alternative mutagenic processes may prevail in the absence of Pol IV.

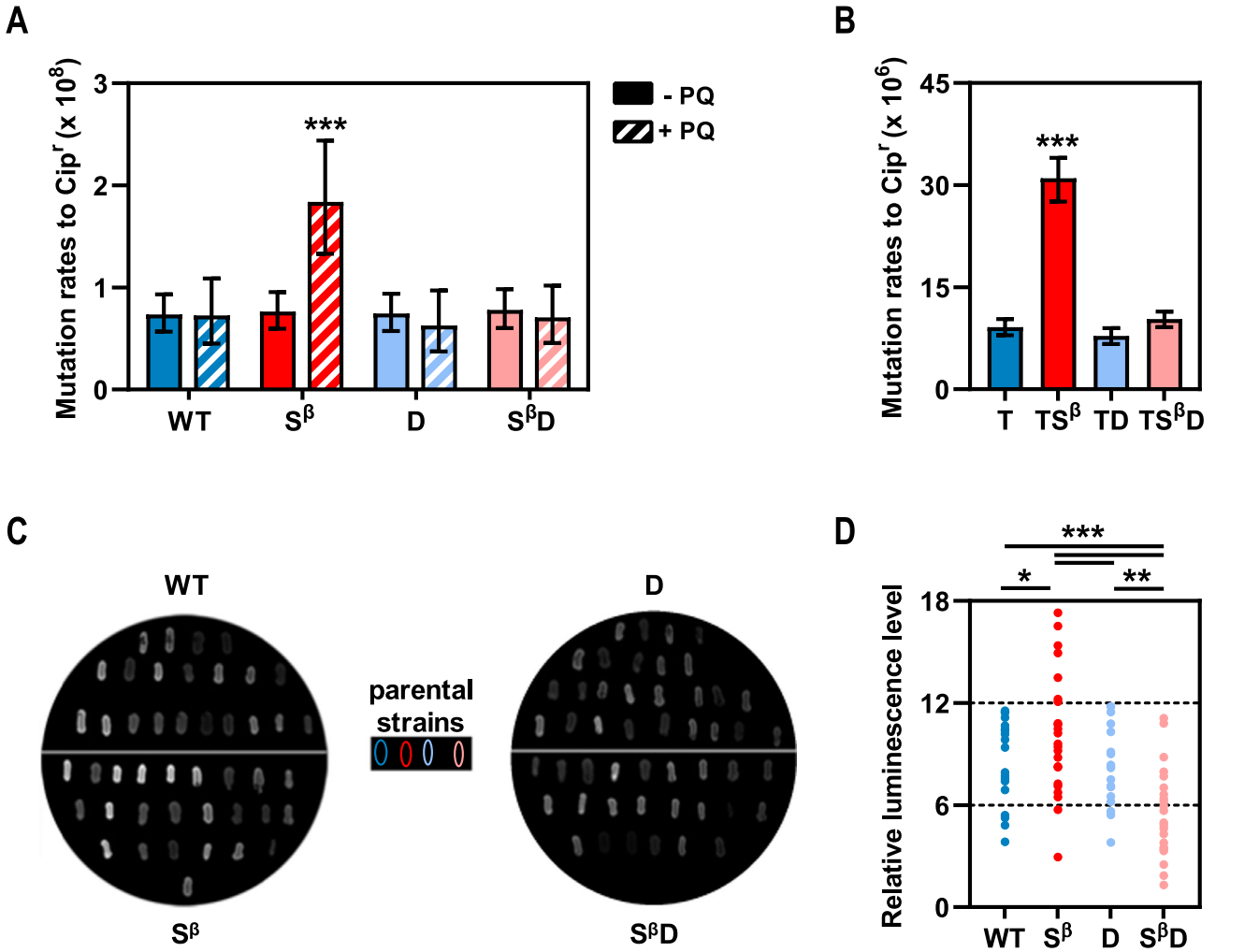

Fig. 1 | Contribution of Pol IV to oxodGTP mutagenesis and gene inactivation. **A** Mutation rates for the wild-type (WT), *mutS*$^\beta$ (S$^\beta$), *dinB* (D) and *mutS*$^\beta$ *dinB* (S$^\beta$D) strains treated (+ PQ) or not (- PQ) with paraquat (40 independent cultures). **B** Mutation rates for the *mutT* (T), *mutT mutS*$^\beta$ (TS$^\beta$), *mutT dinB* (TD) and *mutT mutS*$^\beta$ *dinB* (TS$^\beta$D) strains (20 independent cultures). Mutation rates to ciprofloxacin resistance (Cip^r) per replication and 95% confidence limits were calculated as described in Materials and Methods. Error bars represent the upper and lower 95% confidence limits. Data were statistically analyzed using the likelihood ratio test. **C** Representative images of luminescent Cip^r clones from the WT, S$^\beta$, D and S$^\beta$D strains carrying the chromosomal transcriptional fusion of the *mexCD-oprJ* promoter to the *luxCDABE* operon. **D** NfxB inactivation in Cip^r clones from the WT, S$^\beta$, D and S$^\beta$D strains. Luminescence intensity was measured in exponentially growing cultures of individual Cip^r clones (25–30). The relative luminescence level was calculated as the ratio between the luminescence intensity in the Cip^r clone and the corresponding parental strain. Clones showing luminescence increases of up to 6-, 12- and 18-fold were arbitrarily categorized as expressing NfxB variants with low, medium and high inactivation levels, respectively. Values are the mean from three independent experiments. Results were evaluated using one-way ANOVA and Tukey tests.

The mean number of mutations per line was 74.4, 65.0, 64.4 and 72.8 for T, TS$^\beta$, TD and TS$^\beta$D, respectively (Fig. 2B). Mutations fitted to Poisson distributions ($\chi^2 = 6.2$, $df = 3$, $P = 0.10$), indicating consistent mutation rates throughout experiments, and accumulated in a nearly neutral manner (see Methods and Supplementary Table 6). The spectrum of all strains was dominated by base-pair substitutions (BPSs) (Fig. 2B). BPS rates did not differ significantly between the four groups ($p = 0.42$), averaging 4.16×10^{-9}. This value is 53-fold higher than the genome-wide BPS rate in PA14 (7.92×10^{-11}, Dettman et al.[28]). Importantly, we did not expect a genome-wide increase in mutation rate in the TS$^\beta$ strain, as alternative DNA polymerases like Pol IV have low processivity[4] and do not contribute to the replication of large genomic regions[17].

The BPS spectrum across all strains was biased toward the AT>CG transversion (Fig. 2C and Supplementary Table 7), accounting for 97% of the BPSs ($p = 0.33$, indicating no significant differences among the four strains). This aligns with previous locus-specific experiments in *nfxB* of *P. aeruginosa*[26] and genome-wide analysis in *Escherichia coli*[17]. Nearly all the lines accumulated a single small insertion/deletion (indel, 1-79 bp), occurring at an average rate of 5.32×10^{-11} (Fig. 2B). This rate value is close to that observed in PA14 (1.44×10^{-11}, Dettman et al.[28]). In conclusion, a faulty hydrolysis of oxodGTP exclusively increases AT>CG rates (617-fold, T: 1.32×10^{-8} vs PA14: 2.14×10^{-11}, Supplementary Fig. 4A and Supplementary Table 7), impacting the AT sites in the *P. aeruginosa* genome. Remarkably, this mutational profile is conserved in the four *mutT* strains.

Pol IV is involved in the mutagenesis of specific functional pathways. To assess if Pol IV preferentially targets specific functional pathways, we calculated mutation rates in coding regions across the 27 PseudoCAP functional categories[29], and compared them with the whole-genome mutation rate for each strain to identify deviations (Fig. 3A and Supplementary Table 8). We observed higher mutation rates among genes categorized under "antibiotic resistance and susceptibility", "chemotaxis" and "motility and attachment" in TS$^\beta$. Within these functional categories, we found an enrichment of mutations in genes encoding the Che and Chp chemosensory pathways; structural components of the type IVa pili; structural components of the flagellum and transcriptional

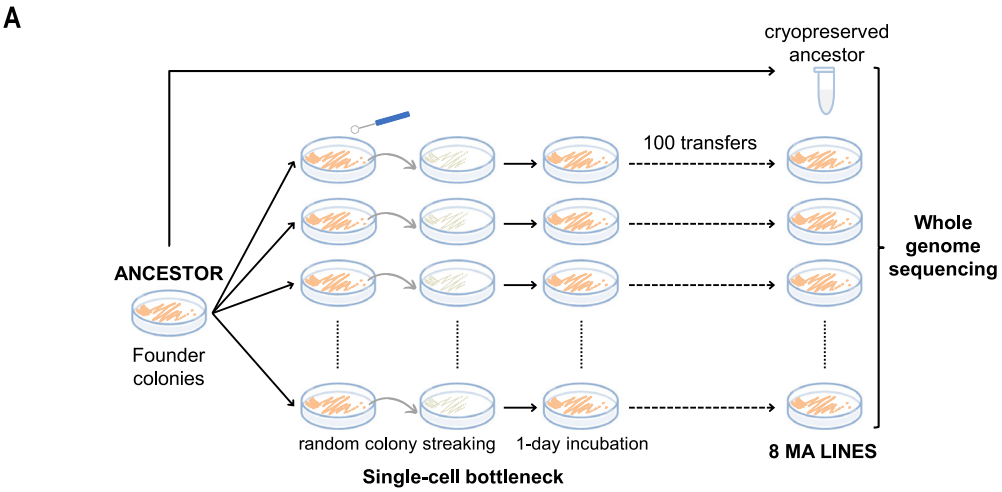

B

Strain	Genotype	BPS per line	BPS rate (x 10^9)	Indel per line	Indel rate (x 10^{11})
T	*mutT*	74.4	4.47 ± 0.38	1.1	6.63
TS$^{\beta}$	*mutT mutS*$^{\beta}$	65.0	3.93 ± 0.42	0.7	4.21
TD	*mutT dinB*	64.4	3.91 ± 0.36	0.9	5.55
TS$^{\beta}$D	*mutT mutS*$^{\beta}$ *dinB*	72.8	4.34 ± 0.35	0.8	4.87

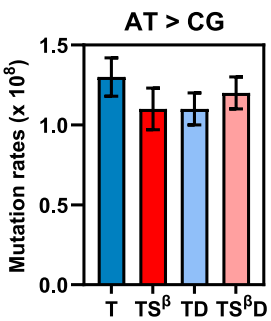

Fig. 2 | Spontaneous mutagenesis in the genome of the *mutT*, *mutT mutS*$^{\beta}$, *mutT dinB* and *mutT mutS*$^{\beta}$ *dinB* strains. A Experimental strategy of the mutation accumulation (MA) experiment. This approach allows mutations to accumulate in a neutral manner with negligible selective pressure. **B** Strain name, genotype, and mutation rates from MA experiments. **C** AT>CG mutation rates. Mutation rates per generation and nucleotide (genome: 6,264,404; AT base pairs: 2,092,311) and 95% confidence limits were calculated as described in Materials and Methods. Confidence limits for values with fewer than 20 mutation events were not calculated due to the lack of statistical power. Plotted data and error bars represent the mutation rate and 95% confidence limits. The data were statistically analyzed using the two-way ANOVA and Tukey tests.

regulators of flagella; and the ATP binding cassette (ABC) and resistance/nodulation/cell division (RND) efflux pumps. None of the PseudoCAP categories showed increased mutagenesis in T, TD and TS$^{\beta}$D. Moreover, although the "membrane proteins" and "secreted factors" categories showed similar mutation rates to the whole-genome (Supplementary Table 8), the genes encoding the outer membrane porins and cytotoxins within these categories were highly mutated in TS$^{\beta}$ but not in T, TD and TS$^{\beta}$D. Mutation rates in these six pathways were 2- to 5-fold higher in TS$^{\beta}$ compared to that observed in T, TD and TS$^{\beta}$D, with the exception of the flagellar genes that also showed a high mutation rate in TS$^{\beta}$D (Fig. 3B and Supplementary Table 9). Mutations in these pathways appeared in 73% of TS$^{\beta}$ lines, averaging 6 mutations per line, while 29% of lines from the other strains had an average of 2 mutations per line (Supplementary Fig. 4B).

In addition, the pyoverdine biosynthesis and secretion pathway, while not differing in mutation rates among the strains (Fig. 3C, Supplementary Fig. 4B and Supplementary Table 9), showed Pol IV-mutation signatures in TS$^{\beta}$ as shown in subsequent data, including most mutations (85%) occurred at sites surrounded by 5' G and/or 3' C and led to gene inactivation. Furthermore, 41 genes associated with other pathways were consistently mutated in TS$^{\beta}$, indicating that they are also Pol IV mutation targets, but not in T, TD and TS$^{\beta}$D. In these genes, 98% of the mutated sites were flanked by 5′ G and/or 3′ C, consistent with Pol IV action. Based on these findings, we identified 96 target genes of Pol IV mutation among the mutational data from the TS$^{\beta}$ lines, comprising 156 mutation events (Supplementary Table 10). These Pol IV-targeted genes and mutations have been pivotal in characterizing the features of Pol IV-induced mutagenesis described in the following sections of this article.

Pol IV mutations are concentrated at specific genome positions. Chromosomal locations could contain mutational hotspots for Pol IV that result in a non-random distribution of mutations along the *P. aeruginosa* genome. To identify preferred genomic targets of Pol IV-mutagenesis, the PAO1 genome was divided into 25 bins of 0.25 Mbp and AT>CG mutation rates were estimated for each bin (Fig. 4 and Supplementary Fig. 5A, and Supplementary Table 11). For all strains, there were no significant differences in mutation rates across the genome. Conversely, Pol IV-induced mutations were not equally distributed along the genome. Three large clusters of mutations appeared at 2.50–2.75 Mbp near the replication terminus region (position ~3.20 M)[30], and at 5.00–5.25 and 5.50–5.75 Mbp close to the rRNA-encoding (*rrn*) genes. In these regions, mutation rates were 4- and 3-fold higher, respectively, compared to those observed for the strains. A fourth cluster was noticed at 0.25–0.50 Mbp, showing a 2-fold increased mutation rate. Remarkably, 94% of pili genes and a substantial proportion (20–70%) of genes involved in pyoverdine biosynthesis, chemosensory pathways, ABC/RND efflux pumps, and porins were located within these four chromosomal regions (Supplementary Fig. 5B). These data indicate a biased distribution of Pol IV-induced mutations towards specific regions of the *P. aeruginosa* chromosome, with the 2.50–2.75 Mbp region exhibiting the highest Pol IV-mutagenic activity.

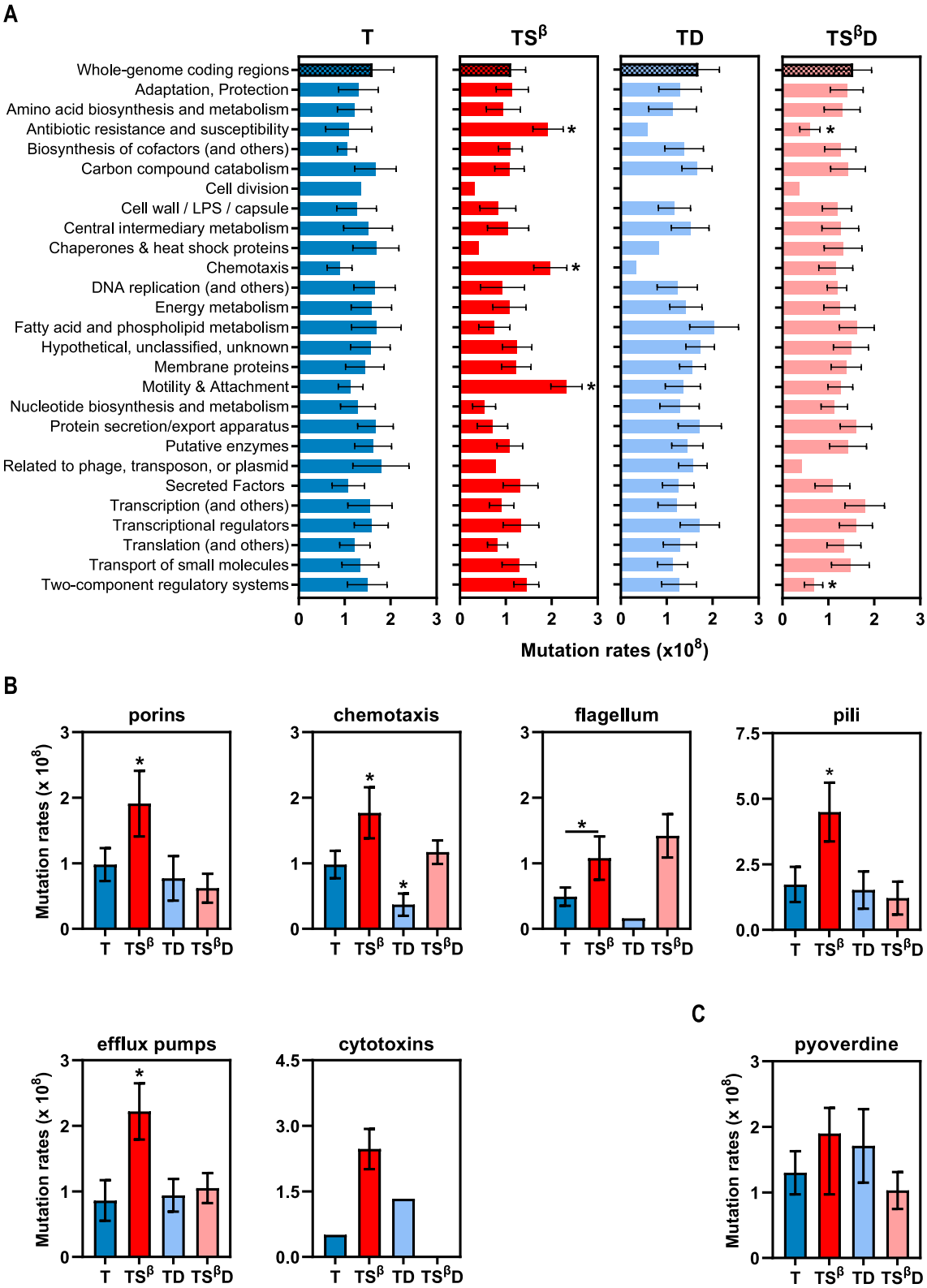

Fig. 3 | Pol IV displays a preference for mutating specific functional pathways. BPS mutation rates in PseudoCAP categories (**A**) and functional pathways (**B**, **C**) for the *mutT* (T), *mutT mutS*$^{\beta}$ (TS$^{\beta}$), *mutT dinB* (TD) and *mutT mutS*$^{\beta}$ *dinB* (TS$^{\beta}$D) strains. Mutation rates per generation and nucleotide of AT>CG mutations (~ 430–670 per founder) in coding regions, and 95% confidence limits were calculated as described in Materials and Methods. The number of AT in the coding regions of the genes included in each PseudoCAP category and functional pathway was used to estimate mutation rates. Confidence limits for values fewer than 5 BPS events were not calculated. Error bars represent the upper and lower 95% confidence limits. No overlap of 95% confidence intervals indicates statistically significant differences. In (**A**), the asterisks show significant differences with the mutation rates in the whole-genome coding regions for each strain. In (**B**), bars marked with an asterisk differ significantly from the others ($p < 0.05$).

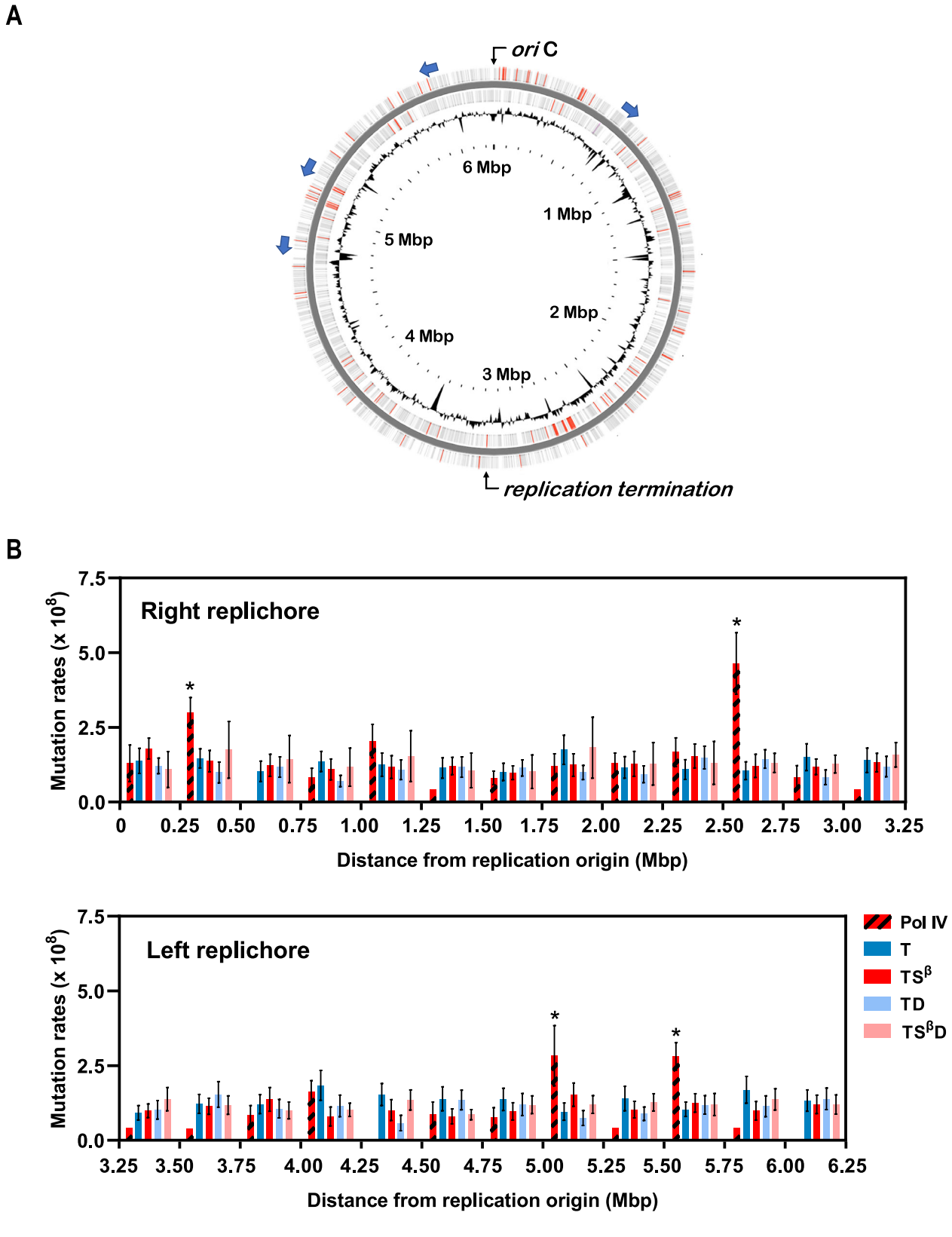

Highly inactive variants are generated by Pol IV in the mutation accumulation assay. We evaluated the ability of Pol IV to generate inactivating mutations under the non-selective conditions of our mutation accumulation experiment. To conduct this analysis, we characterized lines carrying mutations in genes involved in pyoverdine biosynthesis/secretion and flagellum synthesis, for their associated phenotypes. In lines with mutations in the pyoverdine pathway, we quantified the production and secretion of the siderophore (Fig. 5A and Supplementary data 2). Among the 6 TS^{β} lines, 3 showed 20- to 40-fold decreased pyoverdine production compared to the ancestor. None of the 16 lines from T, TD and $TS^{\beta}D$ exhibited reduced pyoverdin production, despite 6 lines had 2 mutations in the pyoverdine pathway. Thus, the 22 mutation events accumulated in these

Fig. 4 | Pol IV-mutational hotspots in the *P. aeruginosa* genome. A Schematic of the PAO1 chromosome. The circular map displays the localization of the origin (*ori*C) and replication termination regions, ribosomal RNA clusters (blue arrows), genes (grey lines) and Pol IV-target genes (red lines). The outer and inner bands represent the plus and minus strands, respectively. The black plot shows the percentage GC content plotted as the average for non-overlapping 0.5 kb windows spanning one strand for the whole genome. The genomic map was generated by Proksee[64]. **B** Mutation rates along the *P. aeruginosa* chromosome. AT>CG mutation rates were plotted as a function of distance from the origin of replication in 0.25-Mbp bins for the Pol IV-target genes and the *mutT* (T), *mutT mutS*$^{\beta}$ (TS$^{\beta}$), *mutT dinB* (TD) and *mutT mutS*$^{\beta}$ *dinB* (TS$^{\beta}$D) strains. For mutation rate calculations, the number of AT > CG per bin was divided by the number of AT in coding regions within the bin and generations. Pol IV-target genes were identified from the mutational dataset of the TS$^{\beta}$ lines. Mutation rates were estimated as the number of AT>CGs per the number of AT in coding regions in each bin and generations. Error bars show 95% confidence limits. Confidence limits for values fewer than 5 BPS events were not calculated. No overlap of 95% confidence intervals indicates statistically significant differences.

strains did not effectively inactivate the pyoverdine genes. Interestingly, 3 lines from T and TD displayed a hyperproduction phenotype. For lines with mutations in flagella genes, we examined swimming motility (Fig. 5B and Supplementary data 2). 50% of TS$^{\beta}$ lines inactivated flagellum synthesis genes. 1 line showed a complete absence of motility and 2 lines exhibited decreased motility compared to the ancestor. Conversely, only 1 line (12%) showed reduced swimming motility, while no significant change was observed in the remaining 7 lines from T, TD and TS$^{\beta}$D. Among these lines, 4 had mutations in 2 to 3 flagella genes, accumulating a total of 12 mutations in the flagella pathway, none of which affected swimming motility. In summary, our data demonstrate that Pol IV is highly proficient at inactivating genes.

Pol IV mutagenesis is biased by the local sequence context. Previous studies using reporter genes showed that Pol IV promotes deletions at mononucleotide repeats and base substitutions at the G**X**C trinucleotide (**X** represents the mutated base)[14,16,31]. We searched DNA sequence preferences for Pol IV by estimating mutation rates for mutated AT nucleotides at each of the 16 possible trinucleotides (Fig. 6A and Supplementary Fig. 6, and Supplementary Table 12). Pol IV significantly promoted mutations at G**A**C + G**T**C and A**A**C + G**T**T, with mutation rates 2- and 3-times higher compared to those observed in T, TD and TS$^{\beta}$D. The mutation rate at G**A**A + T**T**C, associated with oxodGTP mutagenesis[17], was highest among mutations induced by Pol IV and accumulated in the strains. In contrast, A**A**A + T**T**T, A**A**T + A**T**T and T**A**A + T**T**A were not hotspots for Pol IV-induced mutagenesis. Mutations at these trinucleotides were not detected among the Pol IV-mutated genes or exhibited a 2-fold lower value than that observed for the strains.

We next explored the ±10 bp neighboring sequence to identify additional nucleotides influencing Pol IV-mutagenesis using the MEME motif detection algorithm[32]. This analysis did not reveal any conserved sequence context associated with Pol IV-induced mutations. Finally, we investigated if mutated ATs were located outside, adjacent to, between two, or within a mononucleotide repeat (Fig. 6B and Supplementary Table 13). There were no significant differences in the location of mutations induced by Pol IV and accumulated in strains ($p = 0.93$).

Our analysis indicates that a 5' G and/or 3' C surrounding the AT target base is a hotspot for Pol IV mutations at the genome level, consistent with the sequence preference observed in selected mutations of the *nfxB* gene[16]. Conversely, AT sites flanked by T and A bases or located within mononucleotide repeats are not susceptible to Pol IV mutations.

Pol IV preferentially mutates specific codons. We investigated the features of Pol IV-mutagenesis that led to effective gene inactivation. First, we analyzed whether Pol IV has a bias for mutating specific codons by estimating codon mutation rates (Fig. 6C and Supplementary Fig. 7A, and Supplementary Table 14). We noticed a strong preference of Pol IV for mutating GAC, GTC, TCC, GTG and GAA codons, which showed 2- to 4-fold increased mutation levels in Pol IV-mutated genes than that observed for T, TD and TS$^{\beta}$D. In agreement with this, a high proportion of Ser, Val, Asp and Glu were mutated among the Pol IV-target genes (Fig. 6D and Supplementary Fig. 7B, and Supplementary Table 15). Based on this finding, it is expected that mutating AT nucleotides in these codons to CG produces a great proportion of changes to Ala and Gly. Indeed, 24% and 11% of amino acid changes were to Ala and Gly, respectively (Fig. 6E and Supplementary Fig. 7C, and Supplementary Table 15). These proportions were ~2 times higher than those observed in T, TD and TS$^{\beta}$D. Additionally, 55% of mutations involved substitutions among amino acids with charged/uncharged polar and nonpolar aliphatic residues (Supplementary Fig. 7D). These replacements mainly included Glu to Ala, Leu to Arg, Asp to Ala and Ile to Ser. In conclusion, Pol IV preferentially mutates specific codons, favoring shifts to Ala and Gly amino acids and facilitating the change between residues with polar and nonpolar side-chains.

We then investigated if Pol IV has a preference for mutating specific codon positions, leading to nonsynonymous or synonymous mutations. We estimated mutation rates at each codon position for mutations promoted by Pol IV and accumulated across the four strains (Supplementary Fig. 7E). Mutation rates at the three codon positions were similar across all data sets, indicating that Pol IV does not preferentially target specific codon positions.

Pol IV-mutational genomic signatures in clinical isolates of P. aeruginosa

To investigate the potential contribution of Pol IV to bacterial adaptation, we examined single-nucleotide polymorphisms (SNPs) in the *P. aeruginosa* genome of isolates from human infections, including from Cystic Fibrosis patients, and environmental habitats. Clinical and environmental isolates showed 591,087 and 467,429 SNPs, respectively, compared to the PAO1 reference. We first analyzed the SNP distribution across the *P. aeruginosa* genome, divided into 25 bins of 0.25 Mbp (Fig. 7A and Supplementary Fig. 8, and Supplementary Table 16). A wave-like pattern with no significant increase in density in any region emerged for SNPs from clinical and environmental samples. When considering different SNP types, a uniform distribution pattern was evident in transition and transversion SNPs. However, 1.5- to 1.8-fold higher densities were noticed for the four transversions, including AT>CG, in the 2.50–2.75 Mbp region in the clinical isolates but not in the environmental samples. Particularly striking was the enrichment of transversion SNPs in the genome 2.50–2.75 Mbp segment of Cystic Fibrosis isolates, with densities reaching 2.8- to 4.5-fold higher levels. This enrichment was also evident for transition SNPs, albeit to a lesser extent (1.7- to 2.2-fold). In summary, the 2.50–2.75 Mbp region, identified in this study as a Pol IV-target region, serves as a hotspot of diversification among clinical isolates.

Given that this highly variable region includes the Pol IV-target genes for the synthesis and uptake of pyoverdine, we further investigated the 1378 AT>CG SNPs identified within these genes among clinical isolates for evidence of Pol IV-mutagenesis. We analyzed the flanking sequences around AT>CGs (Fig. 7B and Supplementary Table 17), revealing that 68% of SNPs occurred at sites with adjacent 5'G and/or 3'C sequences. Conversely, low occurrences (4%) were found in sequences such as T**A**A + T**T**A, A**A**A + T**T**T, A**A**T + A**T**T and T**A**T + A**T**A. In agreement with these findings, SNPs were notably enriched at codons encoding Glu (GAG and GAA), Asp (GAT and GAC) and Ser (TCG, TCC, TCA and TCT) (Figs. 7C and 7D, and Supplementary Table 17), representing 15%, 11% and 7% of AT>CG occurrences, respectively. Mutation from A to C in these codons often resulted in substitutions to Ala (Fig. 7E and Supplementary Table 17), with 30% of SNPs leading to Ala changes.

In conclusion, our findings reveal Pol IV-mutational signatures within pyoverdine genes from clinical isolates, suggesting that Pol IV may play a role in adaptive mutation processes.

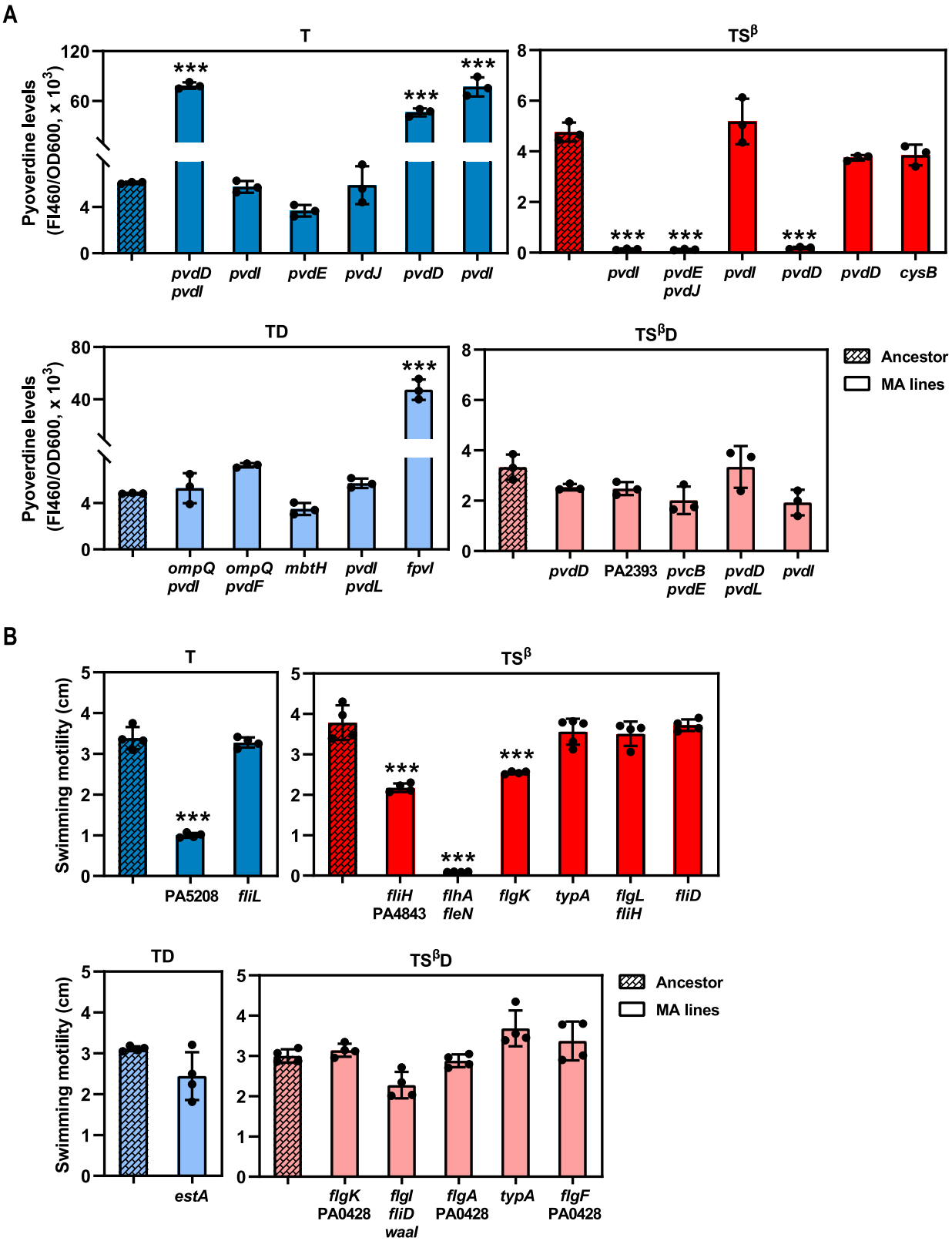

Fig. 5 | Pol IV generates highly inactive variants. A Siderophore production/secretion. Pyoverdine levels were quantified by fluorescence in culture supernatants and normalized to bacterial growth. **B** Swimming motility. Diameters across the zones of bacterial swimming were measured. Bars and error bars represent the means and standard deviations, respectively. The data represent the average of three to four independent measurements. One-way ANOVA followed by Tukey tests were performed to compare each *mutT* (T), *mutT mutS*$^{\beta}$ (TS$^{\beta}$), *mutT dinB* (TD) and *mutT mutS*$^{\beta}$ *dinB* (TS$^{\beta}$D) line with the corresponding ancestral strain. Mutated genes from the pyoverdine and flagella pathways are indicated at the bottom of each MA line bar.

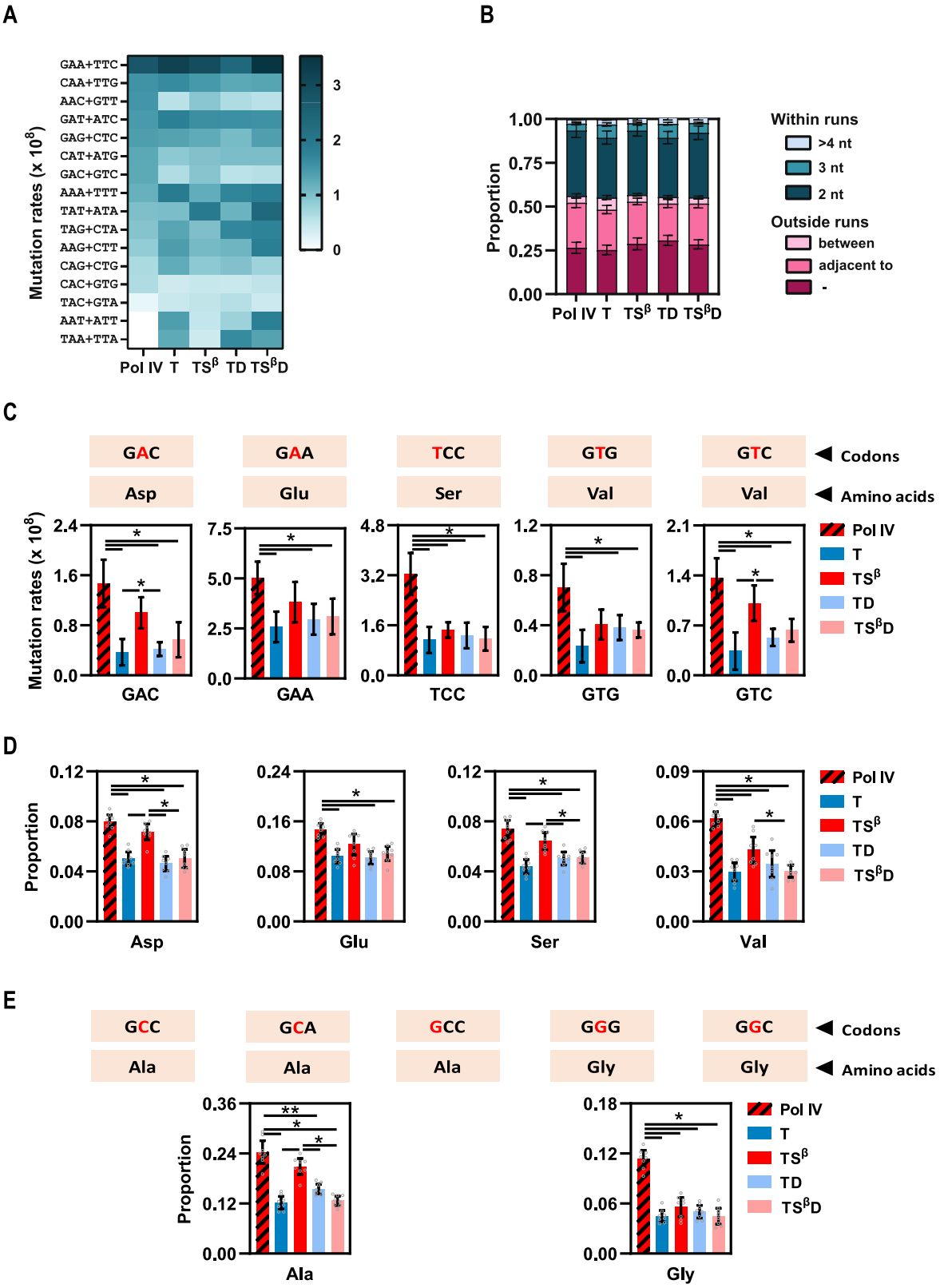

Discussion

We found that Pol IV plays a significant role in the spontaneous mutagenesis of the *P. aeruginosa* chromosome under normal growth conditions. We revealed this mutagenic effect by disrupting the non-canonical function of MutS in controlling Pol IV access to replication sites (*mutS*$^{\beta}$ background)[1,6]. It is important to note that Pol IV-promoted mutagenesis has only been observed in this genetic context in unstressed bacteria. Conversely, Pol IV-mutagenesis has been widely observed in stressed bacteria[10–13]. We hypothesized that this occurs because, during stress, MutS does not regulate the activity of Pol IV. Our previous research demonstrated that Pol IV-promoted mutagenesis is not constrained by the MutS-β clamp interaction under the stress-induced SOS response in *P. aeruginosa*[16]. This suggests that

Fig. 6 | Pol IV has a bias for mutating specific trinucleotides and codons. A BPS mutation rates at trinucleotides. The 5' and 3' bases flanking the mutated nucleotide and their reverse complements were recorded for the AT>CG transversions accumulated in the *mutT* (T), *mutT mutS*$^{\beta}$ (TS$^{\beta}$), *mutT dinB* (TD) and *mutT mutS*$^{\beta}$ *dinB* (TS$^{\beta}$D) strains (422-655 mutations per founder) and induced by Pol IV (151 mutations). Context-dependent mutation rates for mutated AT nucleotides at each of the 16 possible trinucleotides were estimated as the number of mutations at each trinucleotide normalized to the number of this trinucleotide in the genome and generations. Triplets are written 5′ to 3′ with the target site in the center. **B** BPS at mononucleotide repeats. Data bar fill colors indicate the proportion of AT>CGs located outside, adjacent to, between two or within a mononucleotide repeat for mutations accumulated in the Pol IV-mutated genes and the four strains. **C** BPS mutation rates at codons. Mutation rates were estimated for AT>CGs in the Pol IV-mutated genes and accumulated by the T, TS$^{\beta}$, TD and TS$^{\beta}$D strains. Mutation rates were calculated for each codon as the ratio between the number of a mutated codon and the number of that codon in the PAO1 genome and generations. **D**, **E** Amino acid substitutions. The proportion of the target (D) and final (E) amino acids among mutations found in the Pol IV-target genes and accumulated in the T, TS$^{\beta}$, TD and TS$^{\beta}$D strains are plotted. Pol IV-target genes were identified from the mutational dataset of the TS$^{\beta}$ lines. Error bars represent the upper and lower 95% confidence limits for plots of mutation rates. No overlap of 95% confidence intervals indicates statistically significant differences. Error bars represent standard deviations for plots of proportions. The Kruskal-Wallis test was used for the statistical analysis of data.

other factors may regulate MutS activity, or that MutS expression is downregulated under stress conditions. In fact, MutS levels decrease during stationary phase, carbon starvation and exposure to sublethal concentrations of antibiotics, and this depletion promotes Pol IV-dependent mutagenesis[33,34]. To test our hypothesis, we investigated if decreased MutS levels could result in Pol IV-driven mutagenesis (Supplementary Fig. 9 and Supplementary Table 18). Effectively, wild-type *P. aeruginosa* cells with a partial MutS depletion displayed increased Pol IV-dependent mutations under non-stress conditions, supporting the idea that stress-induced downregulation of MutS could trigger Pol IV-promoted mutations.

Our data indicate that the erroneous incorporation of the major product of guanine oxidation in the nucleotide pool underlies Pol IV-mutagenesis, resulting in AT>CG transversions. This agrees with previous biochemical and genetic antecedents. Y-family Pols efficiently incorporate oxodGTP almost exclusively opposite A[8,9,35]. The loss of Pol IV decreases AT>CG levels in sod/fur *E. coli* strains defective for defense against oxidative stress[9], and impairs peroxide-induced mutagenesis in *P. aeruginosa*[7]. Furthermore, our genome-wide analysis revealed no additional mutations flanking AT > CG substitutions. This suggests that Pol IV does not elongate the primer after oxodGTP insertion, leading to untargeted mutagenesis due to its low fidelity synthesis on normal template DNAs[36]. Consistently, *E. coli* Pol IV shows poor extension from primers with a terminal oxodG[37].

Data from this study indicate that MutS recognizes the oxoG:A mispair and shuttle it into an appropriate accurate excision pathway to prevent AT>CG mutations. Indeed, *Helicobacter pylori* MutS and human MutSα bind oxoG-containing DNA duplexes[38,39]. We propose the most likely mechanism for excision of oxoG involves MutS binding to β clamp, which displaces Pol IV from the clamp. This action prevents further nucleotide incorporations by Pol IV and promotes the removal of oxoG through the exonuclease activity of a high fidelity polymerase. Supporting this hypothesis, the exonuclease activities of Pol III and Pol II influence Pol IV-dependent mutagenesis[40,41], and Pol IV overexpression has a stronger mutator effect in *E. coli* cells lacking the exonuclease ε subunit of Pol III[41]. Additionally, inefficient extension of the primer terminus by Pol IV promotes its degradation by the Pol III proofreading activity[42]. Another possibility is that oxoG:A triggers the mismatch repair mechanism. Certainly, Pol IV errors leading to AT>CG mutations are corrected by the MMR in SOS *E. coli* mutator strains[43]. In our experiments, we cannot determine whether the mismatch repair excises oxoGs introduced by Pol IV, as MutS$^{\beta}$ is proficient for mismatch correction[44]. Additionally, the oxoG could be removed by the DNA MutY glycosylase from the GO system. However, we ruled out this possibility because the MutY-catalyzed excision of template A in the oxoG:A mispair could lead to unwanted mutagenesis.

One key finding of this study is that Pol IV-dependent mutagenesis is unevenly distributed across the *P. aeruginosa* chromosome. We identified hotspots for Pol IV activity at specific chromosomal locations, including 0.25–0.50, 2.50–2.75, 5.00–5.25, and 5.50–5.75 Mbp. These regions have similar GC content, trinucleotide composition or codon usage as the entire genome (Supplementary Fig. 10, Supplementary Table 19 and Supplementary data 3), indicating that Pol IV targeting is not influenced by specific features in these DNA sequences. Interestingly, a notable characteristic of these zones is their proximity to replication-challenging regions, such as the replication termination region and the four *rrn* operons. Studies have shown that replication forks arrest at natural or engineered termination sites in *E. coli* and yeast[45,46] and at the highly transcribed *rrn* operons in *B. subtilis*[47]. Furthermore, as observed in our study, chromosomal regions adjacent to these challenging-to-replicate areas are prone to increased genomic instability. Mutation rates are higher around the replication terminus of the *E. coli*, *B. subtilis* and *P. aeruginosa* chromosomes[28,48] and in highly transcribed genes in *B. subtilis* and yeast[49,50].

How does Pol IV target specific genome locations for mutation? We propose that replication stalling in challenging chromosome regions facilitates Pol IV access to replication sites, aiding replication progression. Biochemical studies show that *E. coli* Pol IV is more effective at taking over a stalled Pol III replicase due to nucleotide omission or a blocked replisome caused by a N^2-dG adduct[51,52]. Additionally, Pol IV enriches near replisomes in *E. coli* following methyl methanesulfonate-induced damage[53], and its homolog PoY1 is recruited to stalled forks at highly transcribed lagging-strand genes in *B. subtilis*[49]. Although we described for the first time a preference of a bacterial TLS Pol for mutating replication-challenging genome regions, accumulating evidence suggests similar patterns occur in eukaryotes. *S. cerevisiae* REV1 and Pol ζ-dependent mutations accumulate at sites of replication stalls associated with non-B DNA structures[54].

Another significant finding from this study is the high efficiency of Pol IV for inactivating genes. ~56% of Pol IV-induced mutations in S$^{\beta}$ effectively disrupted gene function under non-selective conditions. Conversely, ~3% of mutations induced by Pol IV-independent mechanisms in the other strains resulted in gene inactivation. Similar results were obtained for Pol IV-induced mutations in the *nfxB* gene selected for antibiotic resistance. We hypothesize that this feature of Pol IV-mutagenesis is attributed to the preference for mutating AT bases surrounded by a 5' G and/or 3' C. Therefore, codons containing these sequence contexts, like GAC, GTC, TCC, GTG, and GAA, are hotspots for Pol IV mutations. Interestingly, these codons are commonly found in the coding regions of *P. aeruginosa* genes, comprising an average of 60% of the total codons used for each encoded amino acid. As Pol IV mutated AT to CG in these codons, most of the changes resulted in substitutions to Ala and Gly. Both amino acids have unreactive side-chains, leading to a significant loss of protein function. Notably, Glu to Ala substitution was the most prevalent Pol IV-induced change (~15%), suggesting that it corresponds to a Pol IV-mutation signature at the amino acid level. In conclusion, Pol IV targets specific amino acids based on its sequence context preference for mutation and changes them to the inert Ala or Gly, effectively causing protein loss-of-function alterations.

Our genomic analysis revealed that Pol IV specifically induces mutations in the chemotaxis, pili, flagellum, efflux pumps, porins, cytotoxins and pyoverdine genes. This finding was consistent with our fluctuation data, suggesting that Pol IV mutagenesis is locus specific in cells growing in colonies. This enzyme effectively induced mutagenesis of the repressor *nfxB* gene, but not of *rpoB* and genes implicated in amikacin resistance. Parallel evolution in the *mutS*$^{\beta}$ lines under the nonselective conditions of the mutation accumulation

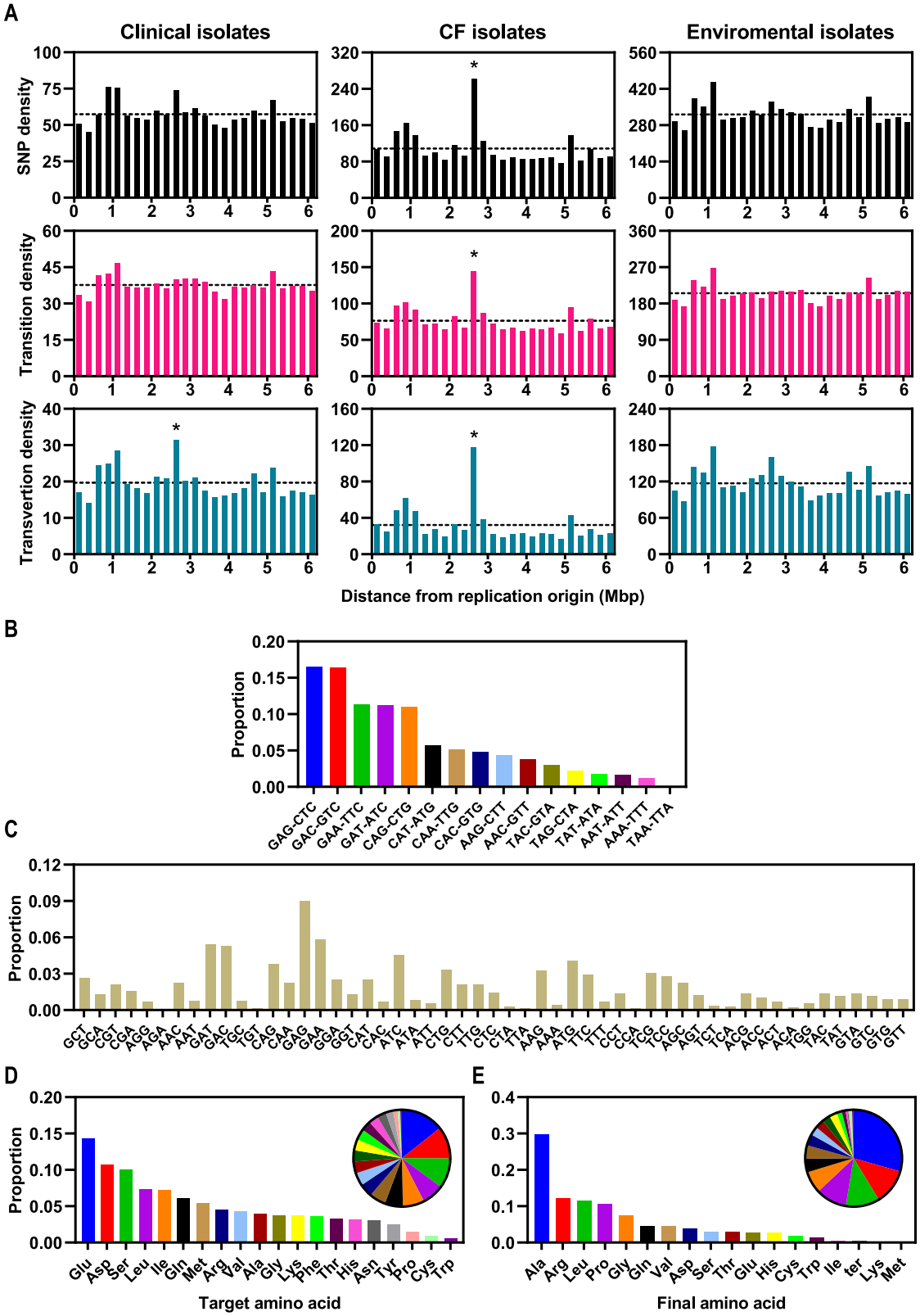

Fig. 7 | Pol IV-mutational signatures on the *P. aeruginosa* genome from clinical isolates. A SNP density plots for the genome of 411 clinical, 59 Cystic Fibrosis (CF) and 58 environmental isolates. The SNP density at each 0.25 Mbp bin was calculated as the total number of SNPs in the bin divided by the number of genomes. Total SNP, transition and transversion densities were plotted as a function of distance from the origin of replication. The dotted line indicates the overall density of SNPs for the chromosome. The Iglewicz and Hoaglin's robust test for multiple outliers (two sided test) was used to detect outlier SNP densities in the genome. Asterisks denote a significant outlier SNP density among genome regions. **B–E** AT>CG mutations in the pyoverdine pathway from clinical isolates. The proportion of mutated trinucleotides (**B**) and codons (**C**); and the proportion of the target (**D**) and final (**E**) amino acids among mutations found in the pyoverdine genes are shown.

experiment could be attributed to the fact that the genes responsible for these traits are located in the Pol IV-preferred genomic regions for mutation. The most evident examples include 70% of pyoverdine genes situated in the 2.50–2.75 Mbp region and 83% of pili genes located in the 5.00–5.25 and 5.50–5.75 Mbp regions. Notably, loss-of-function mutations in these functional pathways are common genetic adaptations found in clinical isolates from chronic lung infections[21,23], suggesting Pol IV could contribute to this genetic diversification of *P. aeruginosa*. The good match between the mutation signatures found in clinical isolates and our experimentally determined Pol IV-mutation profile strongly supports an in vivo role for this mutagenic Pol. We detected Pol IV-mutation signatures in the highly variable 2.50–2.75 Mbp region of clinical genomes, specifically in the pyoverdine pathway. Selected AT>CG SNPs were enriched at sites with neighboring 5'G and/or 3'C and at Glu, Asp and Ser codons. Moreover, these SNPs led to a significant number of changes to Ala, with the Glu>Ala signature being prevalent among amino acid substitutions (~12%).

In summary, Pol IV can accelerate the evolution of pathoadaptive genes located in difficult-to-replicate regions of the chromosome, leading to the generation of highly inactivated variants and enhancing host adaptation. Further investigation is needed to ascertain whether pathoadaptive genes are located in replication challenging regions of bacterial genomes as a common mechanism for rapid evolution through the action of mutagenic DNA polymerases. Based on our findings, we suggest a model for how Pol IV mutagenesis could operate along genomes under stressful conditions (Fig. 8).

Methods

Bacterial strains and culture media

The experiments were carried out using *Pseudomonas aeruginosa* PAO1 and *mutT*::ISphoA/hah (location phoAwp01q3F06) MPAO1 strains. The *mutT* mutator strain was obtained from the University of Washington Genome Center. Transposon insertion within the corresponding gene was confirmed by PCR analysis following the manufacturer's instructions. For the PAO1 and *mutT* MPAO1 strains, isogenic *mutS*$^{\beta}$, *dinB* and *mutS*$^{\beta}$ *dinB* derivatives were made by allelic exchange using the mobilizable suicide plasmid pKNG101[16]. The *mutS*$^{\beta}$ strain harbors a chromosomal *mutS* allele, named *mutS*$^{\beta}$, which codifies a MutS mutant unable to interact with β clamp as the putative β clamp binding ^{816}QSDLF^{820} motif was changed to ASDAA. The *dinB* strain harbors a chromosomal *dinB* allele containing a 753 bp deletion at the 5' of the 1050 bp open reading frame. Luria-Bertani or M9 minimal media were used. To prepare inocula, bacteria were cultured on agar plates from frozen stocks and sub-cultured in liquid LB medium overnight with shaking at 200 rpm at 37 °C.

Estimation of mutation rates by fluctuation assays

Mutation levels of different target genes on the *P. aeruginosa* chromosome were measured by estimating mutation rates to resistance to ciprofloxacin (*nfxB* is mutated at the ciprofloxacin concentration used in this work), rifampicin (*rpoB* is mutated) and amikacin (several target genes are associated to amikacin resistance)[16]. Mutation rates were determined by the modified Luria-Delbruck fluctuation test. Independent cultures (20–40) were obtained as follows: cells were inoculated in LB liquid medium (~500 cells/ml) and grown to exponential phase. For complementation assays, cells freshly transformed with the derivatives of p5BAD were inoculated in LB medium containing 20 μg/ml gentamicin. For paraquat (methyl viologen)-induced mutagenesis, cells were cultured in LB medium amended with 100 μM paraquat. Cell death was negligible under these conditions, and thus, fluctuation assays were conducted. After cultures reached late-exponential phase (~ $0.1–1.0 \times 10^9$ cells/ml), aliquots from successive dilutions were plated onto LB agar or LB agar containing 20 μg/ml gentamicin to determine the number of viable cells, and onto LB containing 0.5 or 1.3 μg/ml ciprofloxacin, 50 μg/ml rifampicin or 2.5 or 10 μg/ml amikacin to select for resistant cells that emerged during exponential growth. Colonies were scored after 16–24 h. The rSalvador program was used to calculate maximum likelihood estimates of m under the Lea-Coulson model, and μ and 95% confidence limits; and to perform the statistical comparison of fluctuation assay data based on the likelihood ratio test.

To estimate mutation rates in cells growing on LB solid media, freshly streaked colonies were grown on LB plates. The number of viable and resistant cells per colony was determined by suspending colonies, diluting and plating onto LB and LB amended with antibiotics, respectively. Each colony was treated as an individual culture in a fluctuation test.

As a control, the minimal inhibitory concentration (MIC) for the antibiotics used in the fluctuation assays was determined according to the guidelines of the Clinical and Laboratory Standards Institute. All strains showed comparable MICs, confirming that the changes in mutation rates were not owing to differences in the MIC.

nfxB inactivation

Inactivation of *nfxB* was analyzed using a luminescent reporter for detection of the transcriptional de-repression of the *mexCD-oprJ* operon[26]. The transcriptional fusion of the *mexC* promoter to the *luxCDABE* reporter operon was inserted into the attTn7 site of the *P. aeruginosa* chromosome using the pUC18-mini-Tn7T-Gm-lux vector[26]. Chromosomal insertions were confirmed by PCR as recommended in the published protocol.

Ciprofloxacin resistant clones were obtained from liquid cultures grown as described in fluctuation assays. Independent clones (25–30)

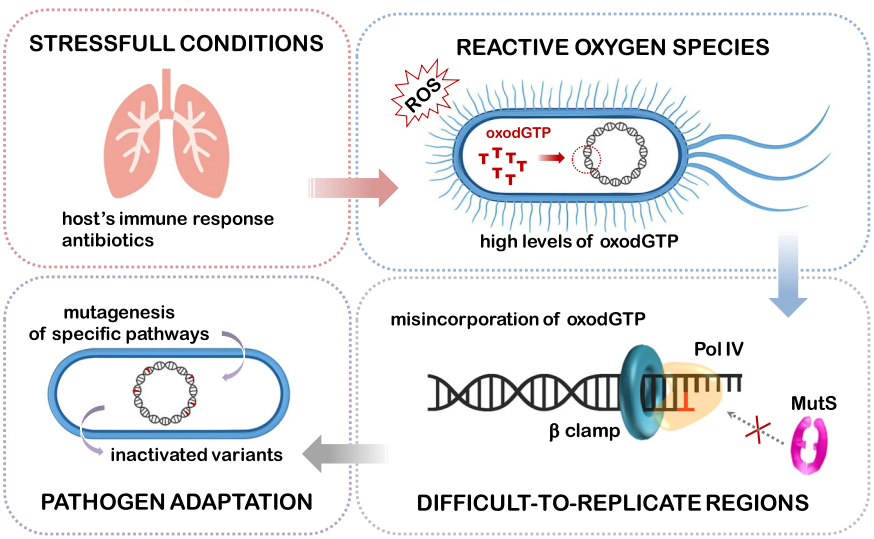

Fig. 8 | Model of Pol IV-mutagenesis across bacterial genomes. Stressful conditions, such those found in the Cystic Fibrosis airway environment, increase the production of reactive oxygen species (ROS), leading to the oxidation of the nucleotide pool. Fork arrest at replication termination sites and highly transcribed zones of the genome facilitates Pol IV molecules enrich near replisomes. This enzyme gains access to the processivity β clamp factor and catalyzes the erroneous insertion of oxodGTP opposite a template A surrounded by a 5'G and/or 3'C. As MutS is unable to regulate the low fidelity DNA synthesis by Pol IV under stress, these errors are fixed as AT to CG mutations. Consequently, Pol IV can drive rapid genomic evolution of genes located in difficult-to-replicate regions of the bacterial chromosome, giving rise to highly inactivated genetic variants that could enhance pathogen survival under hostile conditions.

selected at ciprofloxacin 0.5 µg/ml were picked up onto LB agar plates and then onto LB agar containing ciprofloxacin to confirm that exhibited a stable phenotype.

Luminescence was measured in exponentially growing cells as follows: overnight cultures in LB liquid medium were diluted to an OD 600 nm of 0.1 and seeded in 96-well plates (100 µl). The 96-well plate was then imaged by integrating the luminescence signal for 20 s in a NightOWL LB 983 instrument, and the number of photons emitted per well was quantified using the Berthold WinLight 32 Software. The fold of increase in the luminescence intensity for the ciprofloxacin resistant clones was calculated as the ratio of the number of photons exhibited by cultures of the ciprofloxacin resistant clones and the parental strain.

Ciprofloxacin resistance levels were assessed as follows: overnight cultures grown in LB liquid medium were diluted to ~1000 cells/ml in fresh LB medium, with or without 0.5 µg/ml ciprofloxacin, and dispensed into 96-well plates (100 µl). After incubation for 15 h at 37 °C, bacterial growth was quantified by measuring OD 600 nm. Resistance levels were expressed as the percentage of OD 600 nm values obtained in the presence of ciprofloxacin relative to those from antibiotic-free control cultures.

Mutation accumulation experiments

Lines were initiated from single colonies isolated from *mutT*, *mutT mutS*$^{\beta}$, *mutT dinB* and *mutT mutS*$^{\beta}$ *dinB* strains. The founder colonies were obtained by streaking from a freezer stock onto LB agar plates and incubating the plate overnight at 37 °C. Eight independent well-isolated colonies from each founder strain were streaked out on LB plates and incubated at 37 °C for 24 h. This single-cell bottleneck was repeated 100 times. The colony chosen for passage was the one closest to the end of the streak trace to ensure random selection of colonies. After each transfer, the original plate was stored as a backup plate at 4 °C. If a well-isolated colony was not available for streaking on a particular day, a new streak was made from another colony on the stored plate. The experiment was repeated twice. 8–14 lines of each founder strain were subsequently used for whole genome sequencing.

Prior to initiating the mutation accumulation experiment, we confirmed that all founding strains had comparable fitness in LB medium. No significant differences were observed in maximum growth rates ($p = 0.62$) or colony-forming cell counts ($p = 0.90$) among the four strains. The maximum growth rate during the logarithmic phase of liquid cultures in LB was 1.07 (SD = 0.09), 1.15 (SD = 0.15), 0.93 (SD = 0.07), and 1.14 (SD = 0.26) h^{-1} for *mutT*, *mutT mutS*$^{\beta}$, *mutT dinB* and *mutT mutS*$^{\beta}$ *dinB*, respectively. The average number of cells per colony on LB agar was 1.16 (SD = 0.18), 1.23 (SD = 0.29), 1.19 (SD = 0.31), and 1.25 (SD = 0.36) × 10^8 for *mutT*, *mutT mutS*$^{\beta}$, *mutT dinB* and *mutT mutS*$^{\beta}$ *dinB*, respectively.

Genomic DNA sequencing and variant calling

For whole-genome sequencing of lines, a single colony from the last passage of each mutation accumulation experiment was inoculated in liquid LB and grown overnight with shaking. This culture was used to perform a freezer stock and to extract genomic DNA using the GenElute Bacterial Genomic DNA purification kit (Sigma-Aldrich). Genomic DNA was also harvested from each ancestor strain for sequencing in order to analyze the single nucleotide polymorphisms present prior to initiating the mutation accumulation experiment protocol and filter them from the analysis. Sequence data were obtained from 150 bp, paired-end reads using the Illumina NovaSeq 6000 (Novogene, USA). The mean ± standard deviation of the average depth of coverage across all samples was 190 ± 14. Raw sequence data for the lines and founder genotypes were archived in the NCBI Short Read Archive under BioProject PRJNA1177883.

Raw sequencing data underwent preprocessing using Fastp (version 0.23.2)[55]. This step involved cleaning adaptors, removing bad sequences, and filtering out low-quality sequences to ensure the reliability of subsequent analyses. Cleaned fastq files were aligned to the reference genome using SubRead (version 2.0.1)[56]. Variant Calling was performed using the Genome Analysis Toolkit (GATK) pipeline (version 4.2.5)[57,58]. The BAM file containing aligned reads underwent several steps, including sorting, modifying the read groups, marking duplicates, reordering, and indexing[59]. Annotation of the identified variants was performed using snpEff (version 5.1)[60]. The *P. aeruginosa* PAO1 genome (NCBI Reference Sequence, NC_002516.2; https://www.pseudomonas.com/strain/show?id=107) served as the reference for mapping the variants and providing biological information for interpretation and analysis. This annotation process involved mapping the variants to specific genes, functional regions, and associated biological information, facilitating their interpretation and analysis.

The genome sequence of the founder *mutT* strain differs from PAO1 at 26 single nucleotide polymorphisms (Supplementary Table 20). *mutT mutS*$^{\beta}$, *mutT dinB* and *mutT mutS*$^{\beta}$ *dinB* have additional mutations to that found in the *mutT* strain (Supplementary Table 20). The identity of each line was confirmed by examining the presence of the *mutS*$^{\beta}$ mutation and the *dinB* internal deletion in the *mutS* and *dinB* genes, respectively. For quality control, we verified that mutations specific to founder strains were also called correctly in all descendant lines. The complete set of base substitutions identified in the four founder strains is provided in Supplementary Data 4. A few lines shared some identical mutations, suggesting cross-contamination during passaging. One of the pair of suspect strains was randomly chosen to be discarded from the analysis to ensure each replicate line in the dataset was unique. The mutation dataset was fitted to Poisson distributions. The generalized Pearson statistic and model deviance were used to assess Poisson goodness of fit.

We assessed selection efficiency during line propagation by examining the ratio of mutations in coding versus noncoding DNA (Supplementary Table 6). The expected ratio of mutations in AT nucleotides between coding and noncoding regions in the PAO1 genome is 7.95 under neutral accumulation conditions. In the *mutT*, *mutT mutS*$^{\beta}$ and *mutT mutS*$^{\beta}$ *dinB* strains, the observed ratio was not statistically different from this expectation. The *mutT dinB* strain showed a lower ratio due to an increased proportion of mutations in noncoding regions. This fact is inconsistent with a strong role for selection as selective pressure is assumed to be minimal for noncoding regions. Selective pressure was further evaluated by the ratio of the number of nonsynonymous to synonymous substitutions (Supplementary Table 6). Under the assumption that synonymous mutations are relatively neutral, and given the codon usage in PAO1[61], the expected ratio is 17.47. For all strains, the ratio of nonsynonymous to synonymous mutations did not significantly deviate from this random expectation. These findings collectively support that mutations accumulate in a nearly neutral fashion during the mutation accumulation protocol.

For analysis of *P. aeruginosa* whole-genomes from clinical and environmental isolates, complete genomes were obtained from www.pseudomonas.com/strain and aligned to the reference PAO1 genome using MiniMap2 (version 2.28)[62]. Variant calling was conducted using Bcftools (version 1.15.1)[63]. Annotation of the identified variants was performed using snpEff (version 5.1)[60].

Estimation of generations and mutation rates from mutation accumulation experiments

For each endpoint line and the ancestors, the total number of viable cells per colony was determined by excising colonies from agar plates, re-suspending in LB and plating dilutions on LB agar plates. The number of generations per growth cycle was estimated as the log2 of total cell numbers. The number of viable cells per colony was similar between lines and the corresponding ancestor. Only one line derived from the *mutT mutS*$^{\beta}$ *dinB* strain showed a decrease in the number of viable cells. This line was discarded from the analysis. The mean number of generations per line was 2655 (SD = 51), 2639 (SD = 109), 2631 (SD = 58) and 2673 (SD = 64) for *mutT*, *mutT mutS*$^{\beta}$, *mutT dinB* and *mutT mutS*$^{\beta}$ *dinB*, respectively.

Mutation rates per nucleotide site per cell division were calculated by dividing the total number of accumulated mutations by the total number of generations that the lines passed and by the appropriate number of sites (A:T sites, G:C sites, etc.). Confidence limits (CLs) for the mutation rates

were calculated from the mean and variance of the mutations per line for each strain, using the critical values of the t (student) distribution[18]. The two-way ANOVA test was performed to compare mutation rates between strains after determining normality via the Shapiro-Wilks test and homogeneity of variance via the Levene test.

Phenotypic characterization of lines

Overnight cultures in liquid LB were started from individual colonies of each strain in triplicate. For swimming motility, 2 µl of a 1/10 dilution of overnight cultures was inoculated into the center of Tryptone swim plates (1% tryptone, 0.5% NaCl, 0.3% agar). Plates were incubated at 37 °C for 24 h. Motility was assessed by scanning the plates and measuring the diameter of the circular turbid zone using ImageJ. For pyoverdine quantification, overnight cultures were adjusted to 10^6 cells per ml in M9 minimal medium and incubated with shaking at 200 rpm at 37 °C for 16 h. A 1.5 mL culture was centrifuged at 13,000 rpm for 2 min. 200 µL cell-free supernatants were transferred to a clear-bottom black-side 96-well plate and fluorescence (excitation 360/40 nm; emission 460/40 nm) was measured using a BioTek Synergy HT equipment. Pyoverdine levels were expressed as fluorescence normalized by the biomass of cultures, measured by absorbance (600 nm).

Statistics and reproducibility

Statistical analyses and sample sizes are specified in the figure legends. Analyses were conducted using GraphPad Prism 8.4.3 (GraphPad Software, La Jolla, CA, USA) and the rSalvador package. Statistical significance is denoted as follows: $^*P \leq 0.05$, $^{**}P \leq 0.01$, $^*P \leq 0.001$. Error bars represent the mean ± standard deviation or mutation rates with confidence intervals. All experiments were independently performed at least three times, and quantitative data were derived from a minimum of three biological replicates to ensure reproducibility.

Reporting summary

Further information on research design is available in the Nature Portfolio Reporting Summary linked to this article.

Data access

The data supporting this article can be found in the manuscript and on the Sequence Read Archive (SRA) under the accession number BioProject PRJNA1177883. The numerical source data for Figs. 1 to 7 can be found in Supplementary Tables 1 to 5, 7 to 9 and 11 to 17; and Supplementary data 1 to 4.

Received: 21 January 2025; Accepted: 24 July 2025;
Published online: 02 August 2025

References

1. Horton, J. S. & Taylor, T. B. Mutation bias and adaptation in bacteria. *Microbiology* **169**, 001404 (2023).
2. Kim, Y.-A. et al. Mutational Signatures: From Methods to Mechanisms. *Annu. Rev. Biomed. Data Sci.* **4**, 189–206 (2021).
3. Kaszubowski, J. D. & Trakselis, M. A. Beyond the Lesion: Back to High Fidelity DNA Synthesis. *Front. Mol. Biosci.* **8**, 811540 (2022).
4. Fujii, S. & Fuchs, R. P. A Comprehensive View of Translesion Synthesis in Escherichia coli. *Microbiol Mol. Biol. Rev.* **84**, e00002–e00020 (2020).
5. Putnam, C. D. Strand discrimination in DNA mismatch repair. *DNA Repair* **105**, 103161 (2021).
6. Paniagua, I. & Jacobs, J. J. L. Freedom to err: The expanding cellular functions of translesion DNA polymerases. *Mol. Cell* **83**, 3608–3621 (2023).
7. Sanders, L. H. et al. Epistatic Roles for Pseudomonas aeruginosa MutS and DinB (DNA Pol IV) in Coping with Reactive Oxygen Species-Induced DNA Damage. *PLoS ONE* **6**, e18824 (2011).
8. Katafuchi, A. et al. Critical amino acids in human DNA polymerases η and κ involved in erroneous incorporation of oxidized nucleotides. *Nucleic Acids Res.* **38**, 859–867 (2010).
9. Yamada, M. et al. Involvement of Y-Family DNA Polymerases in Mutagenesis Caused by Oxidized Nucleotides in *Escherichia coli*. *J. Bacteriol.* **188**, 4992–4995 (2006).
10. Sung, H.-M., Yeamans, G., Ross, C. A. & Yasbin, R. E. Roles of YqjH and YqjW, Homologs of the *Escherichia coli* UmuC/DinB or Y Superfamily of DNA Polymerases, in Stationary-Phase Mutagenesis and UV-Induced Mutagenesis of *Bacillus subtilis*. *J. Bacteriol.* **185**, 2153–2160 (2003).
11. Tegova, R., Tover, A., Tarassova, K., Tark, M. & Kivisaar, M. Involvement of Error-Prone DNA Polymerase IV in Stationary-Phase Mutagenesis in *Pseudomonas putida*. *J. Bacteriol.* **186**, 2735–2744 (2004).
12. Kuban, W., Banach-Orlowska, M., Schaaper, R. M., Jonczyk, P. & Fijalkowska, I. J. Role of DNA Polymerase IV in *Escherichia coli* SOS Mutator Activity. *J. Bacteriol.* **188**, 7977–7980 (2006).
13. Niccum, B. A. et al. New complexities of SOS-induced "untargeted" mutagenesis in Escherichia coli as revealed by mutation accumulation and whole-genome sequencing. *DNA Repair* **90**, 102852 (2020).
14. McKenzie, G. J., Lee, P. L., Lombardo, M.-J., Hastings, P. J. & Rosenberg, S. M. SOS Mutator DNA Polymerase IV Functions in Adaptive Mutation and Not Adaptive Amplification. *Mol. Cell* **7**, 571–579 (2001).
15. Sanders, L. H., Rockel, A., Lu, H., Wozniak, D. J. & Sutton, M. D. Role of *Pseudomonas aeruginosa dinB* -Encoded DNA Polymerase IV in Mutagenesis. *J. Bacteriol.* **188**, 8573–8585 (2006).
16. Margara, L. M., Fernández, M. M., Malchiodi, E. L., Argaraña, C. E. & Monti, M. R. MutS regulates access of the error-prone DNA polymerase Pol IV to replication sites: a novel mechanism for maintaining replication fidelity. *Nucleic Acids Res*. **44**, 7700–7713 (2016).
17. Foster, P. L., Lee, H., Popodi, E., Townes, J. P. & Tang, H. Determinants of spontaneous mutation in the bacterium *Escherichia coli* as revealed by whole-genome sequencing. *Proc. Natl. Acad. Sci. USA* **112**, e5990-9 (2015).
18. Foster, P. L. et al. Determinants of Base-Pair Substitution Patterns Revealed by Whole-Genome Sequencing of DNA Mismatch Repair Defective *Escherichia coli*. *Genetics* **209**, 1029–1042 (2018).
19. Niccum, B. A., Lee, H., MohammedIsmail, W., Tang, H. & Foster, P. L. The Spectrum of Replication Errors in the Absence of Error Correction Assayed Across the Whole Genome of *Escherichia coli*. *Genetics* **209**, 1043–1054 (2018).
20. Mulye, M., Singh, M. I. & Jain, V. From Processivity to Genome Maintenance: The Many Roles of Sliding Clamps. *Genes* **13**, 2058 (2022).
21. Winstanley, C., O'Brien, S. & Brockhurst, M. A. Pseudomonas aeruginosa Evolutionary Adaptation and Diversification in Cystic Fibrosis Chronic Lung Infections. *Trends Microbiol.* **24**, 327–337 (2016).
22. Malhotra, S., Hayes, D. & Wozniak, D. J. Cystic Fibrosis and Pseudomonas aeruginosa: the Host-Microbe Interface. *Clin. Microbiol Rev*. **32**, e00138–18 (2019).
23. Camus, L., Vandenesch, F. & Moreau, K. From genotype to phenotype: adaptations of Pseudomonas aeruginosa to the cystic fibrosis environment. *Microbial Genomics* **7**, (2021).
24. Maki, H. & Sekiguchi, M. MutT protein specifically hydrolyses a potent mutagenic substrate for DNA synthesis. *Nature* **355**, 273–275 (1992).
25. Morero, N. R. & Argaraña, C. E. Pseudomonas aeruginosa deficient in 8-oxodeoxyguanine repair system shows a high frequency of resistance to ciprofloxacin: 8-oxodG repair and ciprofloxacin resistance in P. aeruginosa. *FEMS Microbiol. Lett.* **290**, 217–226 (2008).

26. Monti, M. R., Morero, N. R., Miguel, V. & Argaraña, C. E. nfxB as a Novel Target for Analysis of Mutation Spectra in Pseudomonas aeruginosa. *PLoS ONE* **8**, e66236 (2013).
27. Morero, N. R., Monti, M. R. & Argaraña, C. E. Effect of Ciprofloxacin Concentration on the Frequency and Nature of Resistant Mutants Selected from *Pseudomonas aeruginosa mutS* and *mutT* Hypermutators. *Antimicrob. Agents Chemother.* **55**, 3668–3676 (2011).
28. Dettman, J. R., Sztepanacz, J. L. & Kassen, R. The properties of spontaneous mutations in the opportunistic pathogen Pseudomonas aeruginosa. *BMC Genomics* **17**, 27 (2016).
29. Winsor, G. L. et al. Enhanced annotations and features for comparing thousands of *Pseudomonas* genomes in the Pseudomonas genome database. *Nucleic Acids Res*. **44**, D646–D653 (2016).
30. Bhowmik, B. K., Clevenger, A. L., Zhao, H. & Rybenkov, V. V. Segregation but Not Replication of the *Pseudomonas aeruginosa* Chromosome Terminates at *Dif*. *mBio* **9**, e01088–18 (2018).
31. Moyano, A. J., Luján, A. M., Argaraña, C. E. & Smania, A. M. MutS deficiency and activity of the error-prone DNA polymerase IV are crucial for determining *mucA* as the main target for mucoid conversion in *Pseudomonas aeruginosa*. *Mol. Microbiol.* **64**, 547–559 (2007).
32. Bailey, T. L. & Elkan, C. Fitting a mixture model by expectation maximization to discover motifs in biopolymers. *Proc. Int Conf. Intell. Syst. Mol. Biol.* **2**, 28–36 (1994).
33. Gutierrez, A. et al. β-lactam antibiotics promote bacterial mutagenesis via an RpoS-mediated reduction in replication fidelity. *Nat. Commun.* **4**, 1610 (2013).
34. Feng, G., Tsui, H. C. & Winkler, M. E. Depletion of the cellular amounts of the MutS and MutH methyl-directed mismatch repair proteins in stationary-phase Escherichia coli K-12 cells. *J. Bacteriol.* **178**, 2388–2396 (1996).
35. Shimizu, M. et al. Erroneous incorporation of oxidized DNA precursors by Y-family DNA polymerases. *EMBO Rep.* **4**, 269–273 (2003).
36. Kobayashi, S., Valentine, M. R., Pham, P., O'Donnell, M. & Goodman, M. F. Fidelity of Escherichia coli DNA Polymerase IV. *J. Biol. Chem.* **277**, 34198–34207 (2002).
37. Yamada, M. et al. *E scherichia coli* DNA polymerase III is responsible for the high level of spontaneous mutations in *mutT* strains. *Mol. Microbiol.* **86**, 1364–1375 (2012).
38. Wang, G., Alamuri, P., Humayun, M. Z., Taylor, D. E. & Maier, R. J. The *Helicobacter pylori* MutS protein confers protection from oxidative DNA damage. *Mol. Microbiol.* **58**, 166–176 (2005).
39. Mazurek, A., Berardini, M. & Fishel, R. Activation of Human MutS Homologs by 8-Oxo-guanine DNA Damage. *J. Biol. Chem.* **277**, 8260–8266 (2002).
40. Banach-Orlowska, M., Fijalkowska, I. J., Schaaper, R. M. & Jonczyk, P. DNA polymerase II as a fidelity factor in chromosomal DNA synthesis in *Escherichia coli*. *Mol. Microbiol.* **58**, 61–70 (2005).
41. Kuban, W. et al. Mutator Phenotype Resulting from DNA Polymerase IV Overproduction in *Escherichia coli*: Preferential Mutagenesis on the Lagging Strand. *J. Bacteriol.* **187**, 6862–6866 (2005).
42. Foti, J. J. & Walker, G. C. Efficient Extension of Slipped DNA Intermediates by DinB Is Required To Escape Primer Template Realignment by DnaQ. *J. Bacteriol.* **193**, 2637–2641 (2011).
43. Lewis, E. B., Mudipalli, R., Eghbal, M. M. & Culyba, M. J. Effect of mismatch repair on the mutational footprint of the bacterial SOS mutator activity. *DNA Repair* **103**, 103130 (2021).
44. Monti, M. R., Miguel, V., Borgogno, M. V. & Argaraña, C. E. Functional analysis of the interaction between the mismatch repair protein MutS and the replication processivity factor β clamp in Pseudomonas aeruginosa. *DNA Repair* **11**, 463–469 (2012).
45. Larsen, N. B., Sass, E., Suski, C., Mankouri, H. W. & Hickson, I. D. The Escherichia coli Tus–Ter replication fork barrier causes site-specific DNA replication perturbation in yeast. *Nat. Commun.* **5**, 3574 (2014).
46. Bidnenko, V. Replication fork collapse at replication terminator sequences. *EMBO J.* **21**, 3898–3907 (2002).
47. Merrikh, H., Machón, C., Grainger, W. H., Grossman, A. D. & Soultanas, P. Co-directional replication–transcription conflicts lead to replication restart. *Nature* **470**, 554–557 (2011).
48. Niccum, B. A., Lee, H., MohammedIsmail, W., Tang, H. & Foster, P. L. The Symmetrical Wave Pattern of Base-Pair Substitution Rates across the Escherichia coli Chromosome Has Multiple Causes. *mBio* **10**, e01226–19 (2019).
49. Million-Weaver, S. et al. An underlying mechanism for the increased mutagenesis of lagging-strand genes in *Bacillus subtilis*. *Proc. Natl. Acad. Sci. USA* **112**, e1096-105 (2015).
50. Kim, N., Abdulovic, A. L., Gealy, R., Lippert, M. J. & Jinks-Robertson, S. Transcription-associated mutagenesis in yeast is directly proportional to the level of gene expression and influenced by the direction of DNA replication. *DNA Repair* **6**, 1285–1296 (2007).
51. Indiani, C., McInerney, P., Georgescu, R., Goodman, M. F. & O'Donnell, M. A Sliding-Clamp Toolbelt Binds High- and Low-Fidelity DNA Polymerases Simultaneously. *Mol. Cell* **19**, 805–815 (2005).
52. Ikeda, M. et al. DNA polymerase IV mediates efficient and quick recovery of replication forks stalled at N^2-dG adducts. *Nucleic Acids Res*. **42**, 8461–8472 (2014).
53. Chang, S. et al. Compartmentalization of the replication fork by single-stranded DNA-binding protein regulates translesion synthesis. *Nat. Struct. Mol. Biol.* **29**, 932–941 (2022).
54. Northam, M. R. et al. DNA polymerases ζ and Rev1 mediate error-prone bypass of non-B DNA structures. *Nucleic Acids Res.* **42**, 290–306 (2014).
55. Chen, S., Zhou, Y., Chen, Y. & Gu, J. fastp: an ultra-fast all-in-one FASTQ preprocessor. *Bioinformatics* **34**, i884–i890 (2018).
56. Liao, Y., Smyth, G. K. & Shi, W. The Subread aligner: fast, accurate and scalable read mapping by seed-and-vote. *Nucleic Acids Res.* **41**, e108–e108 (2013).
57. De Summa, S. et al. GATK hard filtering: tunable parameters to improve variant calling for next generation sequencing targeted gene panel data. *BMC Bioinforma.* **18**, 119 (2017).
58. Van Der Auwera, G. A. et al. From FastQ Data to High-Confidence Variant Calls: The Genome Analysis Toolkit Best Practices Pipeline. CP *in Bioinformatics* **43**, 11.10.1–11.10.33 (2013).
59. Li, H. et al. The Sequence Alignment/Map format and SAMtools. *Bioinformatics* **25**, 2078–2079 (2009).
60. Cingolani, P. Variant Annotation and Functional Prediction: SnpEff. in *Variant Calling* (eds. Ng, C. & Piscuoglio, S.) vol. 2493 289–314 (Springer US, New York, NY, 2022).
61. Grocock, R. J. & Sharp, P. M. Synonymous codon usage in Pseudomonas aeruginosa PA01. *Gene* **289**, 131–139 (2002).
62. Li, H. Minimap2: pairwise alignment for nucleotide sequences. *Bioinformatics* **34**, 3094–3100 (2018).
63. Li, H. A statistical framework for SNP calling, mutation discovery, association mapping and population genetical parameter estimation from sequencing data. *Bioinformatics* **27**, 2987–2993 (2011).
64. Grant, J. R. et al. Proksee: in-depth characterization and visualization of bacterial genomes. *Nucleic Acids Res.* **51**, W484–W492 (2023).

Acknowledgements

This work was supported by the Secretaría de Ciencia y Técnica (33620230100926CB), Universidad Nacional de Córdoba; and the Agencia Nacional de Promoción Científica y Técnica (PICT 2018-4527).

Author contributions

S.D.C.: Formal analysis, Methodology. C.M.F.: Formal analysis, Methodology. I.N.T.: Formal analysis, Methodology. L.M.M.: Formal analysis, Methodology. M.C.M.: Formal analysis, Methodology. D.G.C.: Formal analysis, Methodology. R.J.P.: Formal analysis, Writing—original draft. M.R.M.: Conceptualization, Formal analysis, Writing—original draft.

Competing interests
The authors declare no competing interests.

Additional information
Supplementary information The online version contains supplementary material available at https://doi.org/10.1038/s42003-025-08589-5.

Correspondence and requests for materials should be addressed to Mariela R. Monti.

Peer review information *Communications Biology* thanks the anonymous reviewers for their contribution to the peer review of this work. Primary Handling Editors: Tobias Goris and David Favero.